

The formation of ordered, ultrathin SiO₂/Si(1 0 0) interfaces grown on (1 × 1) Si(1 0 0)

N. Herbots^{a,*}, J.M. Shaw^a, Q.B. Hurst^{a,1}, M.P. Grams^a, R.J. Culbertson^a,
David J. Smith^a, V. Atluri^b, P. Zimmerman^b, K.T. Queeney^{c,2}

^a Department of Physics and Astronomy, Arizona State University, Tempe, AZ 85287-1504, USA

^b Intel Corporation, Chandler, AZ 85226, USA

^c Bell Labs, Lucent Technology, Murray Hill, NJ 07974, USA

Abstract

Ordering is observed at SiO₂/Si(1 0 0) interfaces when 2–40 nm thick SiO₂ films are grown on passivated, ordered (1 × 1) Si(1 0 0) surfaces produced by a novel wet chemical cleaning. A mechanism is proposed for the occurrence of this ordering. The thin oxides are grown by a variety of conventional oxidation techniques or by rapid thermal oxidation between 750 and 1100 °C. The evolution of oxygen, carbon, hydrogen and silicon coverages are detected by ion beam analysis (IBA) using a combination of ion channeling, nuclear resonance, elastic recoil detection and time-of-flight secondary ion mass spectrometry. IBA detects Si surface peak areal densities lower than that of a disorder-free, bulk-terminated (1 × 1) Si(1 0 0) crystal calculated by Monte-Carlo methods. This result indicates that Si substrate atoms are shadowed by Si atoms located in a 2 nm ordered region on the oxide side of the interface. Beyond 2 nm, the oxide becomes amorphous. Reflection high-energy electron diffraction (RHEED) at 10 keV confirms the presence of order: a (1 × 1) streaky pattern commensurate with Si(1 0 0) is observed instead of an amorphous surface. Infrared (IR) spectroscopy shows that the ordered SiO₂/Si(1 0 0) interfaces exhibit a constant, well-defined frequency of optical absorption across a 1 nm thickness in the interfacial oxide region near Si. This is in contrast to a rapidly changing frequency found for conventional oxides in the same region. Thus, IR supports the presence of a well-defined bond-length and stoichiometry as detected by IBA and RHEED. © 2001 Published by Elsevier Science B.V.

Keywords: Ion beam analysis; Nuclear resonance; Amorphous surface; Ion channeling; Silicon oxide; Crystalline interfaces; SiO₂/Si (100)

1. Introduction

Since the inception of integrated MOS devices, thin silicon SiO₂/Si(1 0 0) has been the material structure of choice to create gate oxides, and SiO₂/Si(1 0 0) has been one of the most studied interfaces. While the bulk of silicon oxide films grown on Si have the well established structure of an amorphous network, the structure and properties of the 0.6–1.5-nm interface between amorphous SiO₂ and crystalline Si(1 0 0) has remained controversial [1–7]. As the scaled down thickness predicted by Moore's law reaches 1–1.5 nm, the thickness of SiO₂

gate oxides is rapidly approaching that of the SiO₂/Si(1 0 0) interface itself (about 1 nm) [7,8]. In parallel, the recent development of so-called 'high-k dielectric' materials as a replacement material for SiO₂ gates is limited by the reactivity of silicon with oxygen. Parasitic formation of an SiO₂/Si(1 0 0) interfacial region limits the gain in capacitance. If Si reoxidation at the interfaces between Si(1 0 0) and these peroxysites or the more conventional oxynitrides is limited, these interfaces present higher electronic interface density of states related to the interface electronic structure, and thus limit to scaling down as well [9,10].

In this paper, the formation of an ordered SiO₂/Si(1 0 0) interface is reported and compared to conventional oxides on Si(1 0 0) from manufacturing sources using three independent techniques: reflection high-energy electron diffraction (RHEED), ion beam analysis (IBA) and infrared (IR) spectroscopy. The properties

* Corresponding author.

E-mail address: nicole.herbots@asu.edu (N. Herbots).

¹ Present address: Utah Valley State College, Orem, UT 84058-5999, USA.

² Present address: Smith College, Northampton, MA 01063, USA.

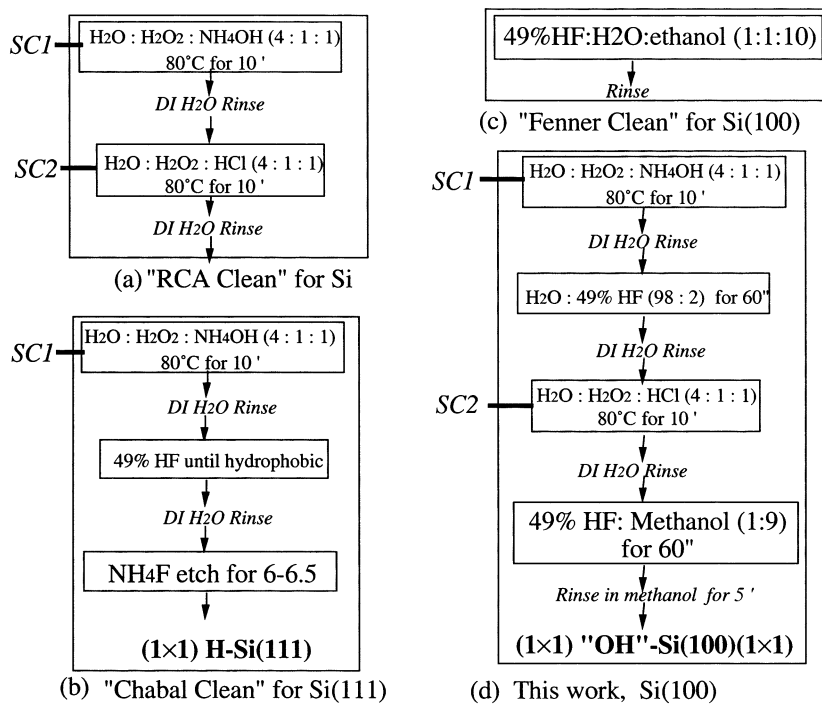


Fig. 1. Three processes ((a)–(c)) whose results led to the design of the process used in this work (d). (a) The ‘RCA clean’ for Si was developed by Kern [13] to remove carbon and oxygen contamination and passivate Si with SiO_2 . (b) The ‘Chabal clean’ orders and passivates by hydrogen termination of Si(1 1 1) without SiO_2 [11]. (c) The ‘Fenner clean’ passivates Si(1 0 0) without SiO_2 and without ordering [16]. (d) This work passivates with OH and orders Si(1 0 0) [17–22].

offered by this new interface are discussed in light of the limitations in thin gate formation of Si(1 0 0) discussed above.

2. Formation of ordered clean Si surfaces stable in ambient air

The initial step in forming an ordered, thin SiO_2 /Si(1 0 0) interface is to create a (1×1) Si(1 0 0) template with good reliability. In the present work, this step is accomplished at room temperature in ambient using wet chemical cleaning in a clean room. A conventional oxidation procedure or else rapid thermal oxidation (RTO) then follows.

Forming a clean, ordered (1×1) Si(1 0 0) surface by wet chemical cleaning at room temperature in ambient air became a research goal after Chabal et al. [11] produced ordered, hydride-terminated (1×1) Si(1 1 1) surfaces which are sufficiently stable in ambient for transfer in air but can be desorbed at $T = 200$ °C. Oxygen does not adsorb on Si(1 1 1) surfaces prepared by this wet chemical cleaning, shown in Fig. 1(b). Called the ‘Chabal clean’, this procedure saturates the highly reactive Si(1 1 1) dangling bonds with H by forming a combination of stable monohydrides, dihydrides and trihydrides [12]. This leads to the formation

of an ordered (1×1) H–Si(1 1 1) surface in ambient. The ‘Chabal clean’ uses the hydrocarbon removal solution (SC1) of the so-called ‘RCA clean’ wet chemical cleaning, outlined in Fig. 1(a) [13], followed by an anisotropic etching in aqueous ammonium fluoride to remove surface domains of orientation other than Si(1 1 1), and a final hydrogenation step in undiluted HF (49%), as shown in Fig. 1(b).

The hydrogenation of Si(1 0 0) is considerably more difficult. Studies on Si(1 0 0) produced hydrogenated Si(1 0 0) surfaces but with considerable roughness, mostly by microfacetting of the Si(1 0 0) plane with Si(1 1 1) domains [14,15]. On the other hand, Fenner et al. [16] reported that silicon dioxide formation could be prevented on Si(1 0 0), without microfacetting of the surface into Si(1 1 1) domains by using aqueous HF (49%) diluted in both ethanol and water in proportion 49% HF:H₂O:ethanol (1:1:10), as shown in Fig. 1(c). In this case, surfaces subjected to ‘Fenner’s clean’ exhibited contamination with C and O lower by an order of magnitude than Si(1 0 0) etched in simple aqueous HF or sputtered with Ar. Surfaces prepared by the so-called ‘Fenner clean’ are stable in ambient for short periods and can be thermally desorbed at temperatures lower than those used for sublimation of SiO_2 but exhibit *no* ordering as observed by low-energy electron diffraction [16].

3. Experimental procedure

3.1. Wet chemical cleaning and analysis prior to oxidation

In the present work, a new wet chemical method cleaning shown in Fig. 1(d) and labeled ‘this work’ was developed by Herbots, Atluri et al. [17–22]. This method can be used to nucleate ordered SiO₂/Si(1 0 0) interfaces. Our wet chemical cleaning produces a Si(1 0 0) surface that is free of silicon dioxide like the surface produced by the ‘Fenner clean’ [16]. However, this Si(1 0 0) surface produced in ambient is also found by electron diffraction to be an *ordered* (1 × 1) Si(1 0 0), unlike the surfaces obtained by Fenner’s clean which did not exhibit any order in the diffraction pattern [16]. This stable, ordered (1 × 1) Si(1 0 0) surface exhibits the typical low desorption temperatures below 600 °C expected for this type of clean [23], leading to reconstruction into a (2 × 1) Si(1 0 0) surface. The 600 °C upper desorption temperature limit is below the 1000–1100 °C temperature for oxide sublimation used in conventional high temperature surface cleaning in ultrahigh vacuum (UHV).

IBA combining ion channeling and nuclear resonance analysis establishes that this stable, ordered (1 × 1) Si(1 0 0) surface is typically terminated by about two monolayers of oxygen and hydrogen [17–19]. The surface is stable up to a few hours in ambient air and does not require storage in nitrogen. An ordered Si/SiO₂ interface can then be formed on these (1 × 1) Si(1 0 0) surfaces, either by letting them oxidize in air for days or weeks [24,31], or by thermal oxidation.

Using the cleaning sequence shown in Fig. 1(d), samples are prepared in a chemical laminar hood, constructed of polypropylene, in a class 100 clean room where a combined ion and molecular beam deposition (CIMD) system is located and RHEED can be performed. The CIMD laboratory clean room itself is located within the IBA for materials facility (IBeAM) at Arizona State University, which thus minimizes the time for transfer and exposure to possible contamination to only a few minutes when samples undergo IBA. The 100-mm diameter B-doped Si(1 0 0) wafers used have a resistivity of 10–14 Ω cm. The ppb grade chemicals are classified as ‘Class 10’ [25].

Thirty percent hydrogen peroxide (H₂O₂) is used for both the so-called ‘SC1’ and ‘SC2’ cleaning solutions annotated in Fig. 1(b) and (d). The tanks for the HF solutions are fabricated with Teflon³. The SC1 and SC2 solutions are heated to 80 °C in Pyrex⁴ glass containers

placed in polyvinylidene fluoride (PVDF) tanks. The PVDF tanks are filled by 18.3 MΩ deionized water and heated by a 4 kW immersion heater controlled by a Microtemp⁵ Controller Model C1115a. The samples are rinsed for 5 min after each step in 18 MΩ deionized water flowing continuously in a tank purged with nitrogen.

3.2. Ion beam analysis

The Si samples used for IBA are 1 × 1 cm² pieces cut manually from a wafer by a diamond scribe in a class 100 laminar hood located in the clean room and transferred immediately between chemical treatments in a Teflon carrier. IBA is conducted in a vacuum of 10^{−8} Torr using a 1.7 MV General Ionex Tandatron accelerator. The signal-to-noise ratio for the detection of oxygen is enhanced by the combination of ion channeling with nuclear resonance analysis. By channeling along a major crystallographic axis in the substrate, the Si background signal can be reduced by about a factor of 30. The sensitivity of RBS to oxygen in the film can be further enhanced by a factor of 27 by adjusting the energy of the incident beam to match the 3.05 MeV ¹⁶O(α,α)¹⁶O nuclear resonance energy [26].

Prior to each ion scattering measurement session, an energy scan is conducted in order to calibrate the ion beam energy to the centroid of the ¹⁶O(α,α)¹⁶O 3.05 MeV ± 5 keV nuclear resonance. Following this calibration, sequential ion channeling measurements are taken. Each successive spectrum is taken without changing the sample’s orientation with respect to the incident beam. This set of spectra measures the O and Si areal density obtained from their respective surface peak (SP) as a function of incident ion dose while accounting for the cumulative damage due to bombardment by the 3.05 MeV He²⁺ analyzing beam. As the total He²⁺ ion dose increases, the apparent areal density of the silicon SP in the oxide layer increases, at the rate expected from the well-established damage rate for He on Si in the MeV range.

By comparing the error bars between a damage curve obtained under channeling conditions and the other obtained while rotating continuously, Fig. 2(a) shows that the signal-to-noise ratio for oxygen is reduced when channeling is used. Using the better sensitivity of channeling, the O areal density from the SP increases with increasing ion dose for a Si(1 0 0) surface cleaned in aqueous HF [20,28,31]. In Fig. 2(b), the slope of the curve for the oxygen areal density is found to be practically equal to zero within statistical error limits for surfaces cleaned via the process developed in this work, as shown in Fig. 1(d). This result establishes that

³ Teflon is a trademark of E.I. Du Pont de Nemours and Company.

⁴ Pyrex is a trademark of Corning Corporation.

⁵ Microtemp is a trademark of Modutek Corporation, San Jose, CA.

no significant oxide growth or desorption occurs during IBA at 10^{-7} Torr on these surfaces. It confirms that these surfaces are fairly stable with respect to reoxidation in ambient air and under lower partial pressure of oxygen. This is not clearly the case for surfaces treated with aqueous HF in Fig. 2(a) where the effect of the IBA is more significant. Fig. 2(b) also establishes that the use of the $^{16}\text{O}(\alpha,\alpha)^{16}\text{O}$ 3.05 MeV improves the signal-to-noise ratio by more than a factor of 4 when compared to 1 MeV channeling [28]. Little shadowing by oxygen atoms is detected at such low coverages, due to the small scattering cross-section of oxygen and the corresponding shadow cone, as well as the significant thermal vibrations of such species [20,27]. Thus, no ion damage can be observed for oxygen in very thin films by channeling while shadowing and damage can be detected for silicon in these films. Thus, a decrease in the Si SP can be expected if ordering is present but cannot be observed in the oxygen SP.

The incident ion dose received by the sample for a Si SP damage curve is up to 30 times greater than that of a single RBS spectrum. This reduces the statistical

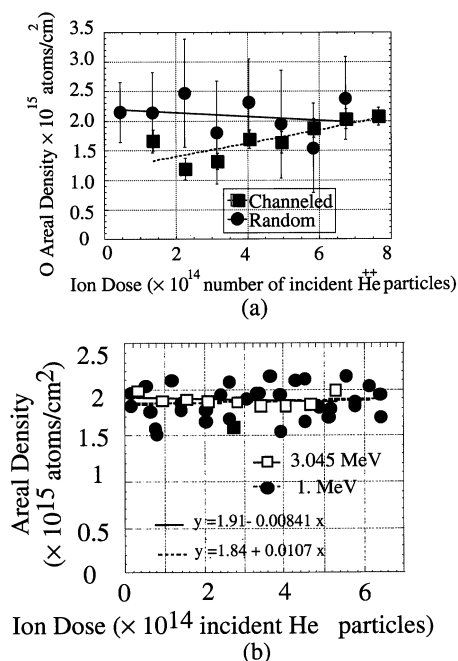


Fig. 2. (a) Example of a so-called ‘damage curve’ obtained by IBA at 3.05 MeV on Si(1 0 0) etched in aqueous HF/H₂O (S3). The O areal density is graphed as a function of the analyzing dose, for eight increments (30 increments were used for the data in Fig. 7). The initial areal density is obtained by taking the intercept of the linear fit. The error bars are much smaller for measurements done in a channeling direction. The positive slope is typical of less stable surfaces processed in aqueous HF [22]. (b) Example of a damage curve obtained on a surface processed by the clean labeled ‘this work’ in Fig. 1(d). Even though 30 increments were used, not a significant slope is noted. The results from the damage curve taken at 3.05 and 1.0 MeV in channeling are statistically identical, but 3.05 MeV exhibits clearly better signal-to-noise ratio.

error. The resulting data is extrapolated by linear least-squares fit to the areal density of an ‘undamaged’ SP and thus the initial oxygen and silicon areal density can be determined [20,22,27,29].

Channeling is conducted in the $\langle 100 \rangle$, $\langle 110 \rangle$ and $\langle 111 \rangle$ directions. More detailed channeling analysis at non-resonant energies, such as 1.0 and 2.0 MeV will be reported elsewhere [29]: these are in agreement with the 3.05 MeV resonance data. They show that the nuclear resonance width of 10 keV includes the entire thickness (≤ 5 nm) of the ultrathin oxide films studied here. Their optical thickness is smaller or equal to 4.5 nm. Thus, the 3.05 MeV resonance provides accurate measurements of oxygen coverages. In each experiment, the set of successive channeling spectra is immediately followed by a succession of ‘rotating random’ spectra. For a rotating random spectra in the direction of the $\langle 110 \rangle$ and $\langle 111 \rangle$ axis, the sample is continuously rotated through a large angular range ($\approx 45^\circ$ and 60° , respectively). For the $\langle 100 \rangle$ case, the sample normal is first tilted away 7° from the beam direction before rotating about the normal. The ratio of the backscattered yield from a narrow region just below the SP in the channeled spectrum to the yield in the same region of the rotating random spectrum is known as the minimum channeling yield χ_{\min} . The χ_{\min} reaches its lowest value of about 0.03 in a perfect Si crystal. Therefore, this ratio measures the degree to which samples are channeled along a crystallographic axis. For every measurement reported here, χ_{\min} was found to be 0.03 or better.

Carbon is detected using a similar methodology by combining ion channeling with the $^{12}\text{C}(\alpha,\alpha)^{12}\text{C}$ 4.265 MeV nuclear resonance. IBA can detect accurately the change in C coverage with each processing step, but the impinging analyzing beam induces the formation of a monolayer of a carbonaceous absorbate via ion-beam-induced deposition [31]. Therefore, time-of-flight secondary ion mass spectrometry (ToF-SIMS) is used to obtain a more accurate value of the final carbon coverage for comparison with standard oxides.

Hydrogen is detected by ERD using $^4\text{He}^{2+}$ at 2.8 MeV and calibrated via the hydrogen signal from a polystyrene standard (C₈H₈). The depletion of hydrogen by the impinging beam due to the recoil is accounted for as a function of the analyzing dose [19]. The effect is minimized by using a small ion dose to measure the standard, while maintaining the statistical counting error to within less than 5% [19].

3.3. Time-of-flight secondary ion mass spectrometry

ToF-SIMS measurements need to be combined with IBA to provide a calibration carbon residue, to determine the magnitude of parasitic buildup during IBA, and to compare carbon incorporation in the films to

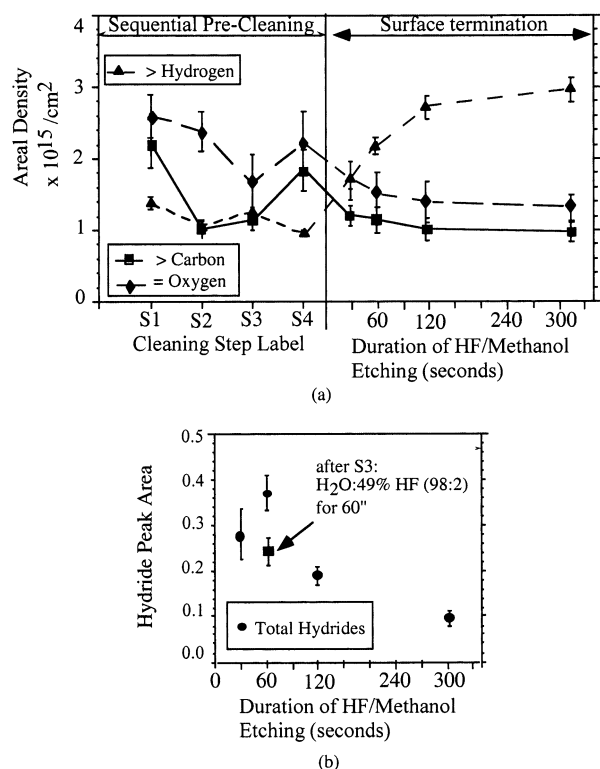


Fig. 3. (a) IBA of surfaces processed sequentially as in Fig. 1(d). The first four steps are labeled S1–S4 (see text) and labeled 'sequential pre-cleaning'. The duration of the last step (S5), labeled 'surface termination' is varied from 30 to 300 s. (b) FTIR–ATR results obtained for S5 (surface termination), showing the relatively small variation in silicon hydrides.

standard thin gate oxides for coverages below the build-up.

ToF-SIMS measurements were made using a Cameca ION-ToF-SIMS 4 instrument in 10^{-10} Torr vacuum. This instrument has a focused gallium low-energy dual-beam sputter gun. This sputter source operates at 400 volts with a beam current of 5 nA. In each measurement, the crater size created by the sputter gun was $200 \mu\text{m} \times 200 \mu\text{m}$ and the SIMS depth profile was taken from a $50 \mu\text{m} \times 50 \mu\text{m}$ window within the crater.

3.4. Reflection high-energy electron diffraction

After introduction of wafers into the UHV system immediately after processing, RHEED diffraction patterns are taken using a 10 keV Perkin–Elmer model 06-190 HEED electron gun in the combined ion and molecular deposition system. The UHV base pressure during RHEED diffraction is 10^{-10} Torr. All images shown are taken with the incident beam angle set at 0.75° to the sample surface plane.

3.5. Infrared spectroscopy

Two different methodologies for IR spectroscopy were used in this work. To assess the formation of hydrides during cleaning, Fourier transform infrared spectroscopy (FTIR) in the attenuation total reflection (ATR) mode is used to detect silicon hydrides (SiH_x). The details of the methodology are reported elsewhere [18,19]. Two hundred and fifty-six scans are co-added to achieve a high signal-to-noise ratio. Samples are referenced against the clean oxide obtained in Step 2 (S2), thus after immersion in the so-called SC1 solution in Fig. 1(b).

The absorption frequencies observed for the different SiH_x species correspond to monohydrides at $2070\text{--}2090 \text{ cm}^{-1}$, dihydrides at $2090\text{--}2120 \text{ cm}^{-1}$, and trihydrides at $2120\text{--}2150 \text{ cm}^{-1}$. Dihydrides and trihydrides are more prominent at 2110 and 2140 cm^{-1} , respectively. Splitting of the dihydride peak is very apparent. Since the goal of the FTIR–ATR experiments was to measure the evolution of the total amount of hydrogen termination chemisorbed on Si and compare it to the net physical coverage of hydrogen atoms, the sum of the three different hydride signals, obtained by adding their respective areas, is reported here.

To assess the bonding at the Si/SiO₂ interface, IR spectroscopy is performed sequentially after thinning the oxide step-by-step using first a surface cleaning followed by etching in dilute aqueous 0.05% HF etching, similar to S2 and Step 3 (S3) in Fig. 1(b). The details of these procedures have been described elsewhere [30].

4. Results and discussion

The evolution of the surface composition is depicted in Fig. 3 (IBA and FTIR–ATR) and Fig. 4 (ToF-SIMS). The evolution of the surface structure is shown by RHEED diffraction in Fig. 5 and compared to high-resolution cross-sectional imaging in Fig. 6 and channeling results in Fig. 7. The pictorial model on Fig. 8 illustrates a possible mechanism for the formation of an ordered oxide interphase on an ordered HO (1×1) Si(1 0 0) surface. This model includes the experimental observations in Figs. 3–7, in our previous work [17–22,27,28] and in other reports [30–34]. Fig. 8(a) and (b) also compare the evolution of the surface morphology in this work to the one found in a typical RCA cleaning sequence.

4.1. O, C and H coverages during the formation of ordered (1×1) Si(1 0 0), SiO₂/Si(1 0 0) interface

The formation of ordered, ultrathin SiO₂/Si(1 0 0) interfaces is initiated in ambient air on ordered (1×1)

Si(1 0 0) surfaces obtained by the wet chemical cleaning sequence shown in Fig. 1(d) labeled ‘this work’. The three other cleaning sequences (Fig. 1(a)–(c)) are shown because their results led to the design of the one used in ‘this work’, and to explain the differences between the surfaces obtained. Fig. 3(a) and (b) show the typical coverage values obtained by IBA and ATR-FTIR over a sampling of 100 wafers measured in 12 separate experiments. The standard deviation on these averages is less than 1.4×10^{14} atoms cm^{-2} for C, and 1.25×10^{14} atoms cm^{-2} for O when measured by IBA on samples processed identically. H coverage is reproducible within 5.5% when measured by ERD.

4.1.1. Initial surface—Step 1

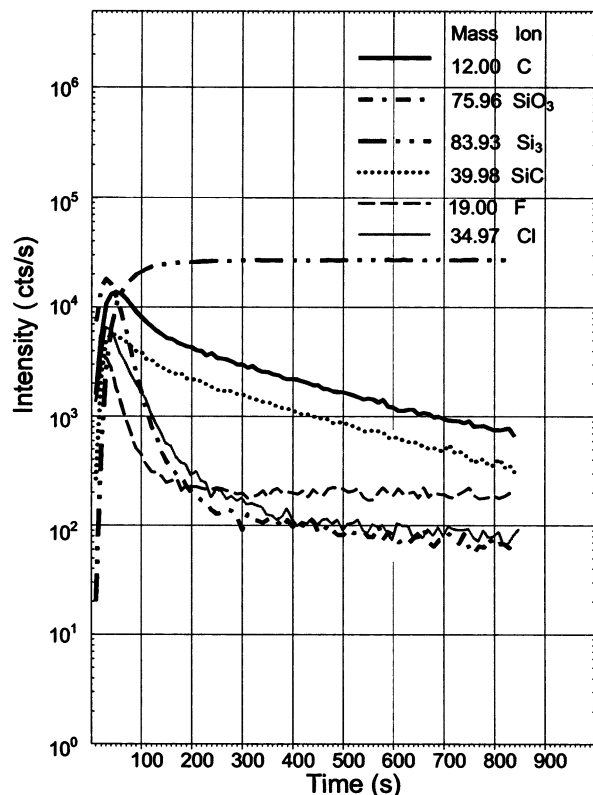
This is the state of the wafer as-received from the manufacturers. The amount of native oxide found in 100 high quality wafers from four different manufacturers typically ranges from a thickness equivalent to 0.8 nm of stoichiometric SiO_2 at the least to 1.6 nm at the most.

4.1.2. Hydrocarbon removal—Step 2

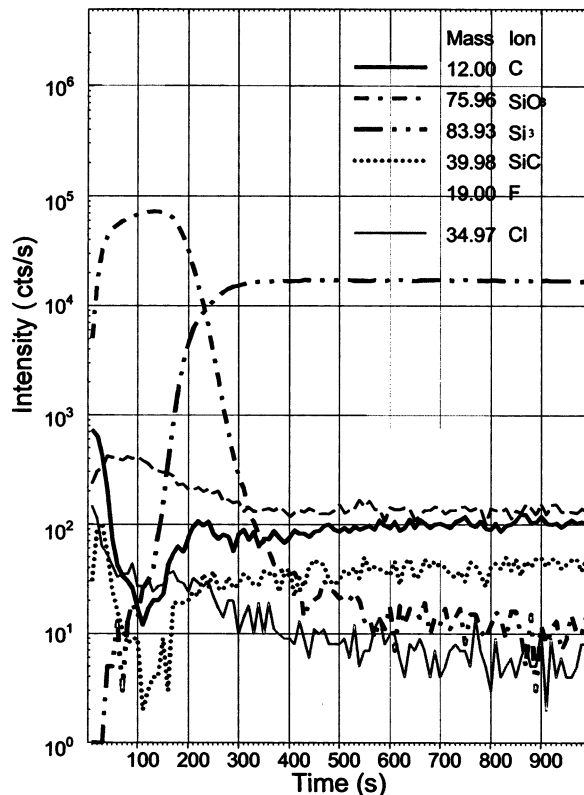
The high pH alkaline SC1 solution with hydrogen peroxide is used first for removing organic and metallic

contaminants, leaving behind the original native oxide, as shown in Figs. 2, 3(a) and 4(a). The SC1 solution used to degrease the wafers has a composition of 4:1:1 parts of $\text{H}_2\text{O}:\text{H}_2\text{O}_2:\text{NH}_4\text{OH}$ where H_2O is 18 M Ω deionized water.

Measurements of carbon and oxygen coverage by IBA after immersion in SC1 are shown in Fig. 3(a) and those show no net oxide growth within an experimental error less than 1.25×10^{14} oxygen atoms cm^{-2} [18,19]. Independent IR measurements of oxide thickness on wafers having undergone a similar SC1 immersion by Queeney et al. [30] also demonstrate that no additional oxide growth occurs in this solution. The lack of oxidation is important prior to the first etching, which in this work immediately follows this one. Absence of oxidation avoids imbedding surface impurities within the native oxide, which happens in the RCA cleaning sequence where an oxidizing step immediately follows, as shown in Fig. 8(a). In the RCA clean, the incorporation of remaining heterogeneities and impurities within the chemical oxide limit the smoothing effect of lateral oxidation by acting as obstacles. The lack of step removal by oxidation prior to the final etching leads to irreversible roughening and disordering.



(a)



(b)

Fig. 4. ToF-SIMS profile for carbon (a) after a surface has been processed by the complete cleaning sequence of Fig. 1(d), and (b) after oxidation by rapid thermal annealing for 90 s at $T = 1050$ °C in pure nitrogen.

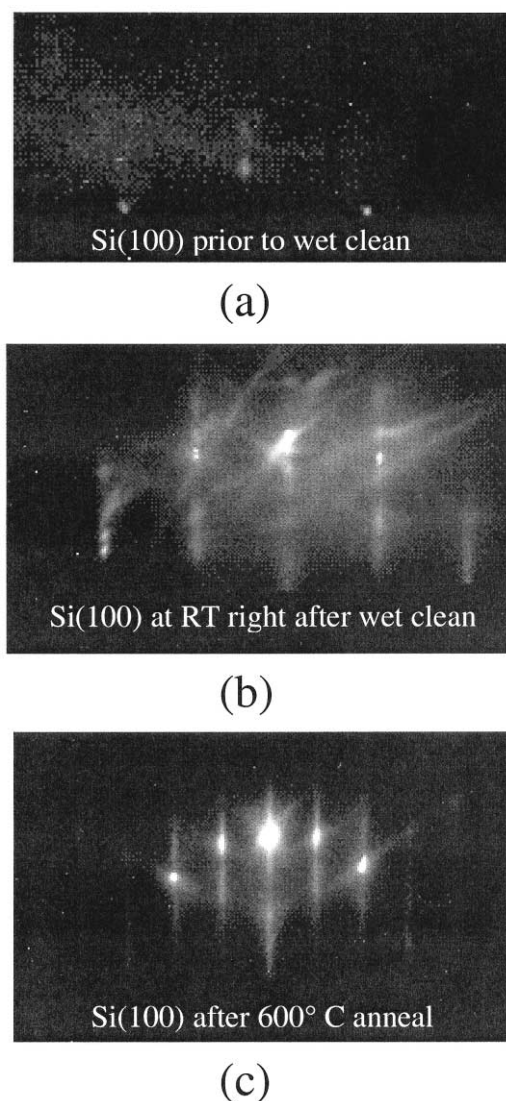


Fig. 5. Typical RHEED diffraction pattern taken at 10 keV on (a) a Si(1 0 0) surface as-received or after having undergone S1–S4, (b) a Si(1 0 0) surface having undergone the complete wet chemical sequence of Fig. 1(d), (c) a Si(1 0 0) surface having undergone the cleaning sequence followed by a 600 °C in situ.

But since no etching of the oxide occurs in S2, no significant roughening occurs, as established by comparative AFM by Atluri [18,19] and independently by Queeney et al. [30]. In fact, Atluri [18,19] observes a very significant decrease RMS roughness when comparing the surface to its initial as-received stage (S1). One order of magnitude decrease in roughness is observed. About half of this decrease is found to be due to particulates, the other half to impurities.

Carbon removal is well known to be the most significant with the SC1 solution, yielding the lowest coverage detected by IBA and other methods. The native oxide is now at its most hydrocarbon-free state with improved smoothness.

4.1.3. Initial oxide removal—Step 3

The hydrocarbon-free native oxide from S2 is then etched away by a conventional 49% HF:H₂O (98:2) aqueous solution for 60 s. Etching in aqueous HF after SC1 immersion yields a uniform rate of removal followed by a uniform reoxidation of the Si(1 0 0) surface. In a classic single-step immersion in HF, hydrocarbon residues form random domains masking oxide regions where the etching rate is significantly reduced [35,36]. This is the cause of the typical surface roughening found in single-step etching. In the cleaning sequence of Fig. 1(d), the resulting surface after S2 and S3 has a thinner, cleaner and more uniform native oxide than the initial surface indicated S1 in Fig. 3(a). It is still amorphous, as shown by RHEED diffraction in Fig. 5. The sample is then rinsed in 18 MΩ deionized water.

4.1.4. Controlled wet chemical reoxidation—Step 4

A new surface oxide is then chemically grown in the acidic hydrogen peroxide SC2 solution [13,18,19] (Fig. 3(a)). The SC2 solution has 4:1:1 parts of H₂O:H₂O₂:HCl. The sample is then rinsed in 18 MΩ deionized water. As depicted in Fig. 8(b), the reoxidation smoothens the surface below the oxide because the high lateral growth rate is not inhibited by imbedded heterogeneities. In the case of the RCA clean [13], the remaining heterogeneities enhance the surface roughness (Fig. 8(a)). The resulting surface exhibits a somewhat enhanced affinity for particulate accumulation, making the use of a clean room critical for this step. Particulate adhesion will interfere with a successful preparation of a uniform Si template.

4.1.5. Final removal of the wet chemical oxide, passivation and rinse—Step 5

The chemically oxidized surface is then etched and passivated by immersion in a solution of methanol and HF diluted in a ratio of 9:1 for 60 s. The final surface is rinsed in methanol, and specifically not in water. A rinse in water dramatically increases the accumulation of surface particulates, obliterating the benefit of the procedure when compared to other cleaning, as observed in this work and other independent studies [17,18,32,33]. In particular, a final rinse in water is found to interfere with the surface ordering in air at room temperature described below

4.2. Surface composition of (1 × 1) Si(1 0 0) before oxidation

The surface coverages of C, H, and O after each cleaning step are measured by IBA and FTIR-ATR and averaged from a study of 90 wafers grouped in nine experimental sets [17,18].

4.2.1. Carbon

When measured by IBA, the amount of carbon is found to decrease to the lowest level detectable, from two to about one monolayer (Fig. 2(a)). This indicates that the cleaning is successful in avoiding an accumulation of hydrocarbon residue. However, since the impinging ion beam induces the formation of a monolayer of carbonaceous absorbate, the IBA needs to be complemented by the more sensitive UHV-based ToF-SIMS, which does not bring about that artifact during analysis. The ToF-SIMS profiles shown in Fig. 4 provide a more accurate comparison of the final carbon coverage of the wet-cleaned Si(1 0 0) with surfaces having undergone conventional cleaning and gate oxides. The carbon ToF-SIMS yield is shown in Fig. 4(a) after passivation in an (1:9) HF:methanol solution and exposure to ambient. This carbon yield is found to be two to three orders of magnitude below the typical coverage found on RCA cleaned wafers before and after oxidation, even several months after processing and extended storage in the clean room.

Thus, the wet chemical cleaning sequence is effective not only in removing carbon residues well below that of standard cleans, but also in reducing the affinity of the resulting surface to carbon build-up. This carbon accumulation is well below the typical build-up found on

uncapped gate oxides, which typically adds an equivalent thickness of about 0.7 nm of material on top of uncapped oxide [33].

This is further demonstrated by the ToF-SIMS profile in Fig. 4(b). A wafer was simultaneously passivated, as in Fig. 4(a), and then oxidized 24 h later by rapid thermal annealing to a thickness of 2.2 nm and left uncapped. The solid line showing the carbon profile in the oxide has dropped by another two orders of magnitude. The carbon concentration remained that low over 12 months. This is in contrast to gate oxides from conventional manufacturing where carbon accumulates within days when the gate oxide is not capped by polysilicon. The added gate thickness due to that carbon accumulation corresponds to a parasitic increase of 30% and cannot be removed without damage to the oxide.

The reduction in C content on the passivated surface and the large reduction in the chemisorption of carbon at the surface are found to exhibit a significant correlation with the lasting structural ordering found before and after the oxides are formed, as described below.

4.2.2. Hydrogen and oxygen

Unlike carbon, oxygen and hydrogen remain in much more significant amounts on the surface when a stable, ordered (1×1) Si(1 0 0) surface is formed.

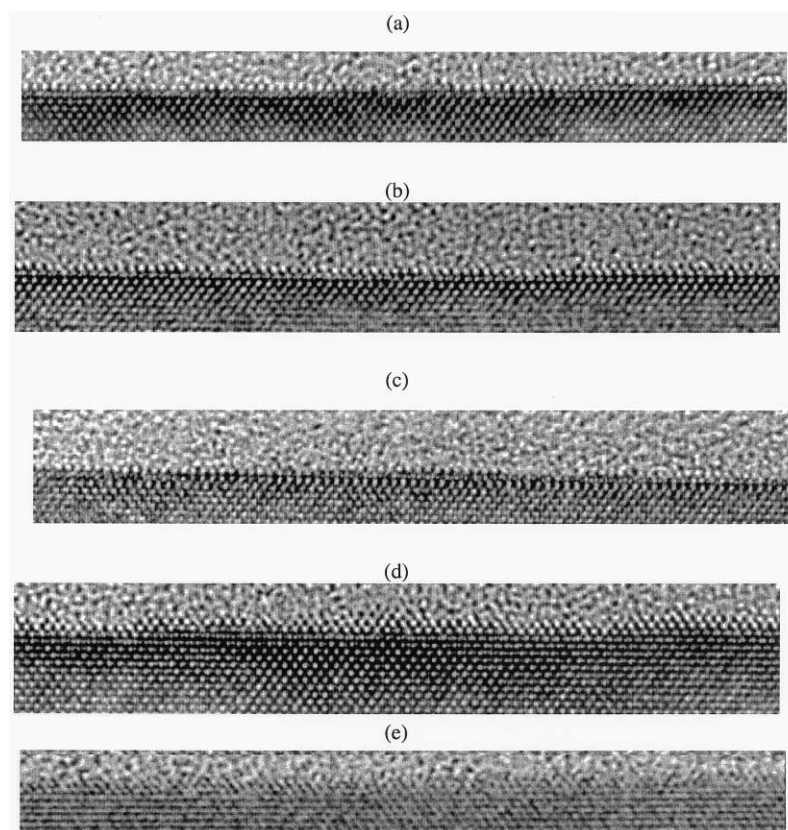


Fig. 6. Cross-sectional HRTEM imaging with a 400 keV JEM 4000 EX and a point resolution = 1.6 Å of three interfacial regions in an ordered oxide ((a)–(c)), and two interfacial regions in a conventional oxide grown on a surface etched with aqueous HF (S3) ((d)–(e)).

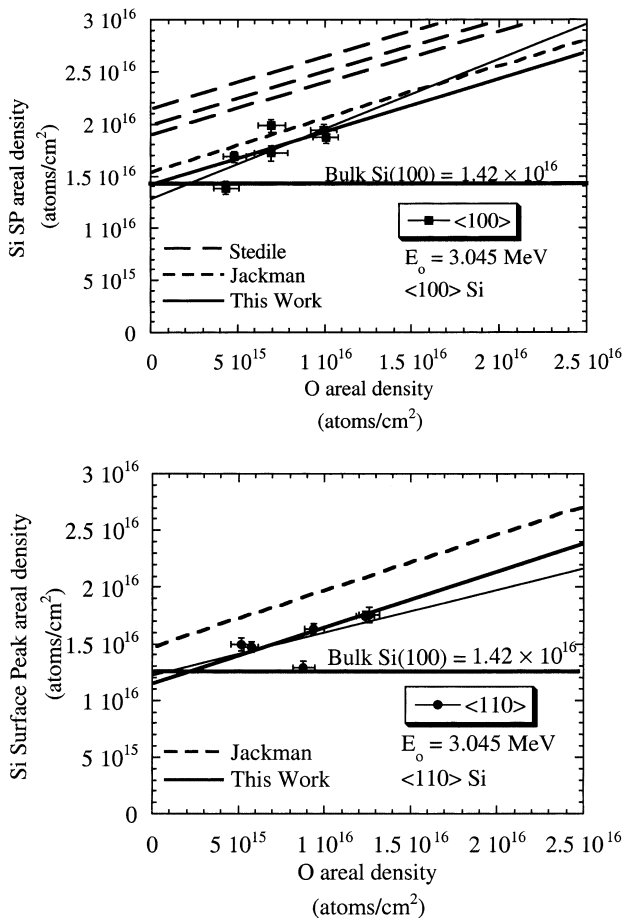


Fig. 7. IBA results for (a) the $\langle 100 \rangle$ channeling direction and (b) the $\langle 110 \rangle$ channeling direction in ordered oxides. A simple linear fit is shown in a fine line, and the fit with a slope of 0.5 (see text) is shown with a thicker line. The results from Refs. [42–46] are shown in thick dashed line for comparison. The Si areal density resulting from the contribution of the bulk crystalline Si SP is shown by the horizontal line.

A decrease in FTIR-ATR absorption for the oxide parallels the decrease in physical oxygen coverage established by IBA after etching in aqueous HF (S3) for 60 s and in HF:methanol for various durations, indicating that most of the SiO_2 is removed by both types of etching. But while the chemical oxide appears almost completely removed, IBA shows that in average about 1.5 oxygen monolayers are detected after both kinds of etching, as seen in Fig. 2(a) and in previous experiments [17]. Thus, 1.5 monolayers of oxygen has to be bonded to a species other than SiO_2 for both etching in aqueous HF (S3) and in HF:methanol (S5). The hydrogen coverage gives a clue about what this species would be in the latter case.

Indeed, the hydrogen coverage is larger by at least a factor of 2 when HF:methanol (1:9) is used. This larger coverage amounts to about two monolayers at the optimum etching duration of 60 s where the best oxide removal, surface ordering and smoothness is observed by streaked RHEED patterns (Fig. 5) and HRTEM in Fig. 6(a)–(c).

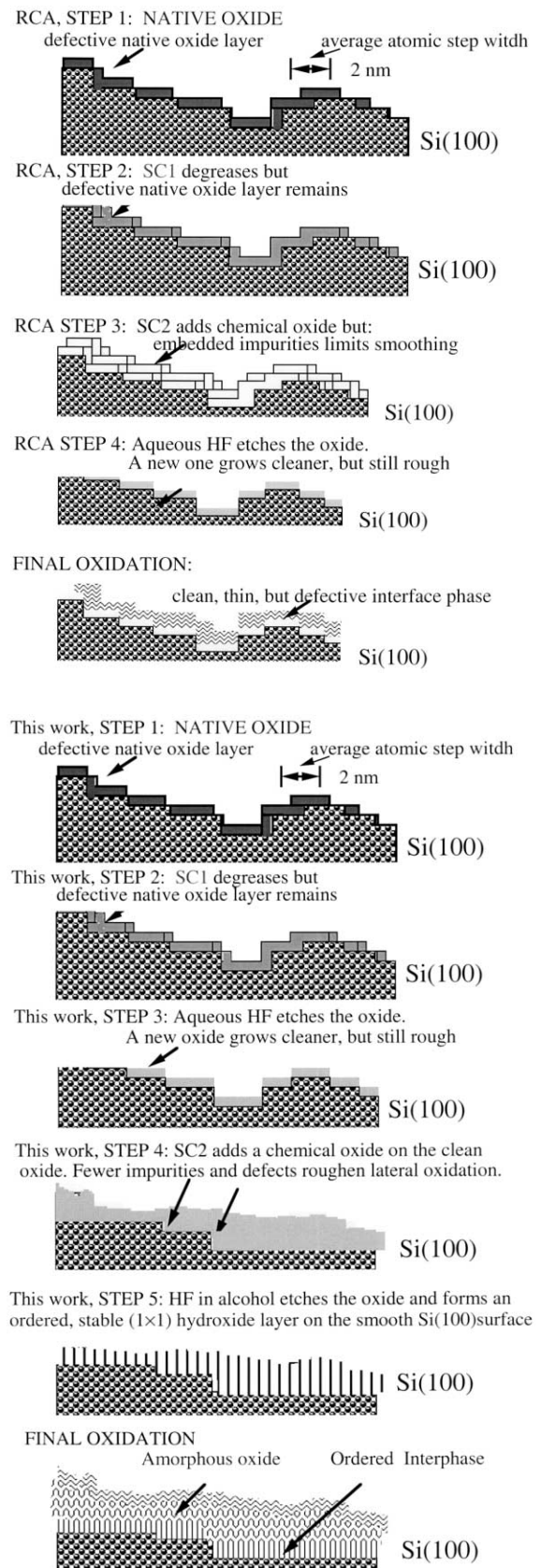


Fig. 8. Model for the surface and its morphology evolution during (a) the RCA clean outlined in Fig. 1(a), and (b) ‘this work’ clean.

Finally, the surface resulting after Step 5 (S5) has unique FTIR adsorption lines [18,19]. In neither of these, the lines are associated with silicon dioxide nor hydrides nor any type of hydrocarbon [12]. Furthermore, the small IR absorption signals found for silicon hydrides decrease when the physical hydrogen coverage is further increased, and do not account for all the hydrogen present, unlike what is observed for H–Si(1 1 1) (1×1) in Ref. [37]. This discrepancy can be seen by comparing the evolution of H coverage measured by ERD in Fig. 4(a) with hydride absorption as a function of etching time in Fig. 4(b). Since the characteristic ratio of hydrogen to oxygen coverage is at least 1:1, the surface obtained after S5 can be annotated OH–Si(1 0 0).

4.2.3. Structure of OH–Si(1 0 0) before and after oxidation into SiO₂/Si(1 0 0)

The OH–Si(1 0 0) surfaces obtained are stable in ambient air at room temperature for an hour or two. Their structure can be examined easily by RHEED by introducing the wafer into UHV and immediately observing the diffraction pattern prior to any thermal processing. Wafers as-received (S1), and up to Step 4 (S4), typically exhibit no diffraction or a faint 1×1 spot pattern from the Si(1 0 0) substrate if the native oxide is thin enough, as can be seen in Fig. 5(a).

In contrast, the RHEED pattern of a wafer that underwent the complete wet chemical process up to S5 exhibits strong (1×1) streaks and spots caused by the ordered termination of the surface. These intense streaked (1×1) patterns show that the surface is smooth and commensurate with the Si(1 0 0) template underneath. The intensity of the streaks and their definition are most pronounced when the pattern is taken within 30 min of the final step of wet chemical cleaning. As hours and days go by, oxidation occurs in air and can be detected by IBA. The RHEED pattern becomes more diffuse but remains streaked for increasing oxygen coverages whereas wafers treated with aqueous HF (S3) exhibits only the faint substrate spots shown in Fig. 5(a). IBA measurements shown in Fig. 7 and discussed below show that the (1×1) surface ordering detected by the characteristic diffraction streaks is maintained in the initial oxide layer. While the faint spotted diffraction pattern in Fig. 5(a) remains unchanged after thermal annealing up to 1000 °C, the RHEED pattern in Fig. 5(b) easily transforms via thermal desorption into the characteristic (2×1) Si(1 0 0) between 500 and 600 °C.

4.3. Oxidation and structure of the SiO₂/Si(1 0 0) interface

4.3.1. Oxidation at room temperature

If the ordered OH–Si(1 0 0) (1×1) wafers are stored

in the clean room, silicon dioxide grows in ambient air linearly with time at an average rate of less than 1×10^{13} atoms cm⁻² day⁻¹ or about 0.5 monolayer per month. Over a period of about 150 days, the typical transition is seen from the linear growth rate associated with the interface reaction being the limiting step to the parabolic rate associated with diffusion-limited growth.

4.3.2. Thermal oxidation between 700 and 1100 °C

A variety of thermal oxidation processes can be used to grow oxides with thickness ranges from 2 to 4 nm and exhibiting ordered SiO₂/Si(1 0 0) interfaces. Both furnace and rapid thermal processing (RTP) can be used, followed by a thermal annealing in nitrogen. Temperatures used ranged between 700 and 1100 °C. At temperatures below or equal to 1050 °C, no significant differences were observed between the interfaces formed, and the interfaces retain the low step density seen in Fig. 6(a)–(c) and exhibit shadowing by ion channeling. At 1100 °C, significant interface roughening was observed by HRTEM.

4.3.3. Structure and morphology of the SiO₂/Si(1 0 0) interface

HRTEM cross-sectional imaging with a 400 keV JEM 4000 EX and a point resolution of 1.6 Å is used in Fig. 6 to compare the difference in interface morphology between oxides. In Fig. 6(a)–(c) oxides grown under identical conditions on ordered OH–Si(1 0 0) (1×1) are shown. Fig. 6(e) and (f) shows the interfaces of oxides grown on Si(1 0 0) having undergone conventional aqueous HF etching in the last step of the cleaning procedure. The key difference observed is the step density and roughness of the interfaces. Surface steps are observed on average every 20 nm in the ~ 10 nm thick cross-sections taken on ordered oxides in the three regions sampled in Fig. 6(a)–(c), whereas they appear every nm in two regions sampled on conventional oxides in Fig. 6(d)–(f). This is a relative measurement since measuring an absolute step density requires a more complex analysis [38–41]. Thus, Fig. 6 shows a relative decrease by an order of magnitude in the observed step density on the surface of ordered oxides. In addition, other quantitative studies of surface roughness by HRTEM conducted under similar conditions can be compared to Fig. 6(d) and (e). These studies [38,39] yield the same step densities and report similar correlation lengths for roughness at conventional SiO₂/Si interfaces as those found here. This indicates that an average projected separation between 1 and 2.5 nm, in such cross-sections is typically observed under the present conditions. The comparison of the morphology in Fig. 6(a)–(c) with recent images of SiO₂/Si interfaces in a quantitative study also indicate that they have an unusual degree of smoothness [41]. Finally, the smooth morphology found for ordered oxides in Fig. 6(a)–(c) is

also in agreement with the dominant two-dimensional surface geometry associated with streaked RHEED diffraction pattern in Fig. 5(b).

The structure of the interface cannot be deduced unambiguously from HRTEM. Interference from the substrate structure near the interface cannot be conclusively separated from the contrast observed in the film [1,3]. However, IBA can detect unambiguously alignment of Si atoms within the oxide with respect to the Si atoms of the substrate.

Fig. 7(a) and (b) and Table 1 summarize the results for the structural analysis of SiO₂/Si(1 0 0) interfaces by IBA. Fig. 7 shows the areal density obtained from the Si SP as a function of oxygen coverage in the <1 0 0> direction in Fig. 7(a), and in the <1 1 0> direction in Fig. 7(b). The intercept of a linear plot for zero oxygen coverage has been used to measure disorder at the SiO₂/Si(1 0 0) interface by several researchers [42–46]. The slope for the linear plot is typically set at a value of 0.5 to match the known stoichiometry for silicon dioxide. While this simple model ignores the details of the interface structure, it provides a straightforward comparison between different oxides. In addition, in this work, each data point in Fig. 7 is an areal density obtained from a damage curve, such as the one shown in Fig. 2 by taking the intercept for a null analyzing dose. By measuring the evolution of the Si SP yield as a function of oxygen coverage one can detect whether subsequent oxide layers are registered with the substrate.

Indeed, the Si SP as measured by RBS is a sum of backscattered yield from three regions: (1) the intrinsic bulk Si(1 0 0) SP in the crystalline substrate, (2) the Si SP in the interface region and (3) Si atoms in the bulk of the oxide films (unregistered with respect to the substrate). Monte-Carlo simulations [47] are used to calculate the bulk-terminated Si(1 0 0) substrate areal densities [20,42–47]. The measured Si SP areal density is marked B in Table 1. The calculated bulk Si SP for a perfect Si(1 0 0) crystal is marked A in Table 1. The difference B–A is marked C in Table 1. A positive difference has always been reported [42–47] ranging from at least one and a half monolayer of disordered Si, and up to 11 monolayers of disordered Si. The amount of disorder has been shown to depend on the preparation procedure used [40,41,46]. Our results with the same analysis, however, show no such disorder at the interface. The intercepts for the <1 0 0> and <1 1 0> directions are slightly below the expected value for bulk Si(1 0 0), within the experimental error, as shown in Table 1. For further comparison, lines with a slope of 0.5 and an offset equal to the different amount of disorder reported in Refs. [42–46] are shown in Fig. 7. These demonstrate that the SP reported fall below the experimental values corresponding to previous report.

4.4. Infrared spectroscopy results

IR spectroscopy should, in principle, be an ideal technique to study this interface since it is extremely sensitive to the details of local bonding configuration. However, interpretation of the broad spectral features inherent to amorphous SiO₂ is difficult and therefore controversial. A novel approach has been developed [30] to extract details of the structure of ultrathin SiO₂ from IR spectra. The TO frequency for the ordered oxides is found to be higher by several wave numbers throughout the thickness analyzed (2.5 nm). In particular, the TO frequency drops only three wave numbers, from 1059 cm⁻¹ at 1 nm to a constant value of 1057–1056 cm⁻¹ in the first 0.4–1 nm of the oxide region. Conventional oxides show a more pronounced and continuous decrease of the LO frequency by six wave numbers from 1059 to 1052–1053 cm⁻¹ starting at 1 nm from the interface within the same 0.4–1 nm region. The LO frequencies are also found to be higher within 1.25 nm from the interface, falling from 1240 cm⁻¹ at 1 nm to 1216 cm⁻¹ at 0.4 nm. The conventional oxides exhibit a redshift from 1235 cm⁻¹ at 1 nm to 1213 cm⁻¹ at 0.4 nm. This comparison shows that ordered oxides exhibit a more constant, better defined frequency of optical absorption across a 1 nm thickness in the interfacial oxide region near the Si substrate. This result is in contrast to a rapidly changing frequency found in conventional oxides in the same region. Thus, IR supports the presence of a well-defined bond-length and stoichiometry as detected by IBA and RHEED. A detailed analysis of the IR data will be reported elsewhere [48].

5. Conclusions

A new Si(1 0 0) surface process using wet chemical cleaning has been developed and found to yield a clean, ordered Si(1 0 0) surface stable in air at room temperature with an average oxygen incorporation rate of less than 10⁸ O cm⁻² sec⁻¹. This relative stability is sufficient to permit the transfer of wafers in atmosphere for further processing without significant disordering or reoxidation. The surface is found by RHEED to be reconstructed as (1 × 1) Si(1 0 0) and unusually two-dimensional for a passivated Si(1 0 0), which are usually found to be three-dimensional. A combination of IBA, including oxygen resonance and hydrogen recoil, and FTIR-ATR indicate that the surface is covered by several monolayers of hydrogen and oxygen in similar proportion, with relatively few silicon hydride bonds when compared to a native oxide. This suggests that the surface is likely to be terminated as OH–Si(1 0 0) (1 × 1). After oxida-

Table 1
Comparison between amounts of disordered silicon found in previous reports and this work

Ion channeling energy (MeV)	Si(1 0 0) orientation; crystal axis	A = calculated bulk Si(1 0 0) SP; $\times 10^{15}$ atoms cm^{-2}	B = measured Si SP; $\times 10^{15}$ atoms cm^{-2}	C = B – A = net disorder in Si; $\times 10^{15}$ atoms cm^{-2}	Equivalent disordered Si monolayers; $\times 10^{15}$ atoms cm^{-2}	Reference	Initial surface process	Oxidation
0.8	$\langle 110 \rangle$	6.4	8.6	2.2	2.3	[44]	Aqueous HF	Furnace
0.8	$\langle 100 \rangle$	7.6	9	1.4	2.1	[45]	Not reported	1000 °C furnace
0.8	$\langle 110 \rangle$	6.4	8.6	2.2	2.3	[45]	Not reported	1000 °C furnace
0.8	$\langle 100 \rangle$	7.6	15	7.4	10.9	[46]	RCA	1050 °C RTO
0.8	$\langle 100 \rangle$	7.6	13.6	6	8.8	[46]	HF in ethanol	1050 °C RTO
0.8	$\langle 100 \rangle$	7.6	12.9	5.3	7.8	[46]	Rapid thermal cleaning	1050 °C RTO
3.05	$\langle 100 \rangle$	14.2	14	–0.2	0.0	This work	Section 4.1	Section 3
3.05	$\langle 110 \rangle$	12.5	11.5	–1	0.0	This work	Section 4.1	Section 3

The table shows the reported values (marked B) for the intercepts obtained from areal density curves, such as the ones shown in Fig. 7 from Refs. [42–47] and the amount of disorder detected from these measurements (marked C). These are then compared to the ones measured here.

tion by various conventional processes at temperatures below 1100 °C, the interface formed exhibit unusual properties: the topography of the interface remains highly two-dimensional and the step density measured by HRTEM along the interface is an order of magnitude lower than the density measured on conventional Si(1 0 0)/SiO₂ interfaces IBA detects no disorder at Si/SiO₂ interfaces formed on OH–Si(1 0 0) (1 × 1), in contrast to all previous reports on conventional oxides [42–46]. Both IBA and RHEED data indicate that the ordered oxide interphase is significantly commensurate with the Si(1 0 0) substrate. These results confirm the findings in [42–46] that the amount of unregistered atoms found at the interface is affected by the initial surface processing. Finally, IR spectroscopy also shows smaller redshifts near the interface; also suggesting that bonding exhibits a more defined geometry than in conventional interfaces.

Based on these observations, a mechanism is proposed to describe the evolution of the morphology leading to the formation of ordered SiO₂/Si(1 0 0) interfaces. The conditions of formation of this interphase require that the initial interface be formed at low temperature and that step density and number of domain boundaries be small, in agreement with the recent model proposed in Ref. [49]. Further characterization is being pursued to establish the structure and compare it to recent calculations on ordered SiO₂/Si(1 0 0) interfaces [49], and other experiments, such as epitaxial SiO₂/Mo(1 1 2) [50–52] and crystalline SiO₂ precipitates in Si [53].

Acknowledgements

The authors wish to thank Y. Chabal for his willingness to share his expertise in the area of Si(1 1 1) surface physics and processing early in this project and his interest for this work on Si(1 0 0). His support in conducting IR analysis at Lucent is gratefully acknowledged. Access to RTO, furnace oxidation and electrical characterization at Intel Corporation was arranged by Dr Brian Doyle for Justin Shaw during his Master's thesis research and is here gratefully acknowledged. Intel Corporation provided financial support under grant donation ASUF133-1220 and the Research Corporation provided financial support under Grant no. RA0256. M. Grams was supported by REU NSF Grant no. DMR-9531053 when performing this work. Electronic-grade Si(1 0 0) wafer donations arranged by R. Swift and F. Wilson, Motorola Inc., Semiconductor Products Sector, Phoenix, AZ, and by Dr Brian Doyle, Intel Corporation are gratefully acknowledged. General Chemicals, Pittsburgh, CA, provided support for some of the class 10 clean room chemicals in the initial phase of this project. Technical assistance provided by B. Wilkens in the IBA for materials facility (IBeAM) at ASU is also gratefully acknowledged.

References

- [1] A. Ourmazd, D.W. Taylor, J.A. Rentschler, J. Beuk, *Phys. Rev. Lett.* 59 (2) (1987) 213.
- [2] A.C. Diebold, D. Venables, Y. Chabal, D. Muller, M. Weldon, E. Garfunkel, *Mater. Sci. Semicond. Process.* 2 (2) (1999) 103.
- [3] G.Y. Fan, J.M. Cowley, J.C.H. Spence, *Phys. Rev. Lett.* 58 (3) (1987) 282.
- [4] (a) P.J. Grunthaner, M.H. Hecht, F.J. Grunthaner, N.M. Johnson, *J. Appl. Phys.* 61 (2) (1987) 629;
(b) P.J. Grunthaner, F.J. Grunthaner, R.W. Fathauer, T.L. Lin, M.H. Hecht, L.D. Bell, W.J. Kaiser, F.D. Schowengerdt, J.H. Mazur, *Thin Solid Films* 183 (1989) 197.
- [5] Y. Tu, J. Tersoff, *Phys. Rev. Lett.* 84 (19) (2000) 4393.
- [6] R. Buczko, S.J. Pennycook, S.T. Pantelides, *Phys. Rev. Lett.* 84 (5) (2000) 943.
- [7] J.B. Neaton, D.A. Muller, N.W. Ashcroft, *Phys. Rev. Lett.* 85 (6) (2000) 1298.
- [8] G. Lucovsky, Y. Wu, H. Niimi, V. Misra, J.C. Phillips, *Appl. Phys. Lett.* 74 (14) (1999) 2005.
- [9] J.C. Phillips, *J. Vac. Sci. Technol.* B17 (4) (1990) 1803.
- [10] G. Lucovsky, H. Yang, H. Niimi, J.W. Keister, J.E. Rowe, M.F. Thorpe, J.C. Phillips, *J. Vac. Sci. Technol.* B18 (3) (2000) 1742.
- [11] G.S. Higashi, Y.J. Chabal, G.W. Trucks, K. Raghavachari, *Appl. Phys. Lett.* 56 (7) (1990) 656.
- [12] V.A. Burrows, Y.J. Chabal, G.S. Higashi, K. Raghavachari, S.B. Christman, *Appl. Phys. Lett.* 53 (11) (1988) 998.
- [13] (a) W. Kern, *RCA Rev.* 31 (1970) 187;
(b) W. Kern, *Curr. Cont./Eng. Technol. Appl.* 11 (1983) 18.
- [14] V. Le Thanh, D. Bouchier, G. Hincelin, *J. Appl. Phys.* 87 (8) (2000) 3700.
- [15] T.H. Bok, J.H. Ye, S.F.Y. Li, *J. Vac. Sci. Tech.* A18 (5) (2000) 2542.
- [16] D.B. Fenner, D.K. Biegelsen, R.D. Bringans, *J. Appl. Phys.* 66 (1) (1989) 419.
- [17] V. Atluri, N. Herbots, D. Dagel, S. Bhagvat, S. Whaley, *Nucl. Instr. Meth. Phys. Res.* B118 (1996) 144–150.
- [18] V. Atluri, N. Herbots, D. Dagel, H. Jacobsson, M. Johnson, R. Carpio, B. Fowler, *Mater. Res. Soc. Symp. Proc.*, in: G.S. Higashi, M. Hirose, S. Raghavan, S. Verhaeverbeke (Eds.), *Science and Technology of Semiconductor Surface Preparation*, vol. 477, 1998, p. 281.
- [19] (a) V. Atluri, *Hydrogen passivation of Si(1 0 0) used as templates for low temperature epitaxy & oxidation*, Ph.D. Thesis, University of Arizona and Arizona State University, 1998;
(b) N. Herbots, V. Atluri, J. Xiang, J.D. Bradley, S. Banerjee, Q.B. Hurst, US patent filed.
- [20] N. Herbots, V. Atluri, Q. Hurst, J.M. Shaw, S. Banerjee, J.D. Bradley, R.J. Culbertson, D.J. Smith, *Mater. Res. Soc. Symp. Proc.*, in: S. Ashok, J. Chevallier, K. Sumino, B.L. Sopperi, W. Goetz, R.C. Bowman (Eds.), *Defect and Impurity Engineered Semiconductors and Devices II*, vol. 510, 1999, p. 157.
- [21] V. Atluri, N. Herbots, *Mater. Res. Soc. Symp. Proc.*, in: N.H. Nickel, W.B. Jackson, R.C. Bowman (Eds.), *Hydrogen in Semiconductors and Metals*, vol. 513, 1999, p. 399.
- [22] Q.B. Hurst, N. Herbots, J.M. Shaw, M.M. Floyd, D.J. Smith, R.J. Culbertson, M.P. Grams, J.D. Bradley, P. Zimmerman, V. Atluri, *Mater. Res. Soc. Symp. Proc.*, in: H.R. Huff, M.L. Green, T. Hattori, G. Lucovsky, C.A. Richter (Eds.), *Ultrathin SiO₂ and High-K Materials for ULSI Gate Dielectrics*, vol. 567, 2000, p. 183.
- [23] D.J. Eaglesham, G.S. Higashi, M. Cerullo, *Appl. Phys. Lett.* 59 (6) (1991) 685.
- [24] M.P. Grams, *Proceedings of the Research Experience for Undergraduates at Arizona State University*, 1998, p. 100.

- [25] All chemicals are from General Chemicals, Pittsburgh, CA. Pharmaceutical reagent grade ethanol, manufactured by EM Science Corp. was provided by Alameda Scientific, Phoenix, AZ.
- [26] J.A. Leavitt, L.C. McIntyre Jr., M.D. Ashbaugh, J.G. Oder, Z. Lin, B. Dezfouly-Arjomandy, *Nucl. Inst. Meth. B44* (1990) 260.
- [27] Q.B. Hurst, Ph.D. Thesis, Arizona State University, 2000.
- [28] J.M. Shaw, M.Sc. Thesis, Arizona State University, 2001.
- [29] N. Herbots, J.M. Shaw, Q.B. Hurst, R.J. Culbertson, D.J. Smith, unpublished results.
- [30] K.T. Queeney, M.K. Weldon, J.P. Chang, Y.J. Chabal, A.B. Gurevich, J. Sapjeta, R.L. Opila, *J. Appl. Phys.* 87 (3) (2000) 1322–1330.
- [31] S. Banerjee, M.Sc. Thesis, Arizona State University, 1998.
- [32] M.Y. Hao, K.F. Lai, W.M. Chen, J.C. Lee, *Appl. Phys. Lett.* 65 (9) (1994) 1133.
- [33] G.B. Alers, D.J. Werder, Y. Chabal, H.C. Lu, E.P. Gusev, E. Garfunkel, T. Gustafsson, R.S. Urdahl, *Appl. Phys. Lett.* 73 (11) (1998) 1517.
- [34] P.J. Zimmerman, Intel Corporation, private communication, 1998.
- [35] P. Allongue, C.H. de Villeneuve, S. Morin, R. Boukherroub, D.D.M. Wayner, *Electrochim. Acta* 45 (28) (2000) 4591.
- [36] H. Sakaue, S. Fujiwara, S. Shingubara, T. Takasago, *Appl. Phys. Lett.* 78 (3) (2001) 309.
- [37] M. Copel, R.J. Culbertson, R.M. Tromp, *Appl. Phys. Lett.* 65 (18) (1994) 2344.
- [38] D.A. Muller, T. Sorsch, S. Moccio, F.H. Baumann, K. Evans-Lutterodt, G. Timp, *Nature* 399 (1999) 758.
- [39] F.H. Baumann, C.-P. Chang, J.L. Grazul, A. Kamgar, C.T. Liu, D.A. Muller, *Mater. Res. Soc. Symp. Proc.*, in: L. Clevenger, S.A. Campbell, B. Herner, J. Kittl, P.R. Besser (Eds.), *Gate Stack and Silicide Issues in Silicon Processing*, vol. 611, in press.
- [40] Z. Liliental, O.L. Krivanek, S.M. Goodnick, C.W. Wilmsen, *Mat. Res. Soc. Symp. Proc.*, in: J.M. Gibson, L.R. Dawson (Eds.), *Layered Structures, Epitaxy, and Interfaces*, vol. 37, 1984, p. 193.
- [41] S.M. Goodnick, D.K. Ferry, C.W. Wilmsen, Z. Liliental, D. Fathy, O.L. Krivanek, *Phys. Rev.* B32 (1985) 8171.
- [42] L.C. Feldman, S.T. Picraux, *Materials Analysis by Ion Channeling*, Academic Press, New York, 1982.
- [43] L.C. Feldman, J.W. Mayer, S.T. Picraux, *Fundamentals of Surface and Thin Film Analysis*, North Holland, New York, 1986.
- [44] N. Cheung, L.C. Feldman, P.J. Silverman, I. Sternsgaard, *Appl. Phys. Lett.* 35 (1979) 859.
- [45] T.E. Jackman, J.R. MacDonald, L.C. Feldman, P.J. Silverman, I. Stensgaard, *Surf. Sci.* 100 (1980) 35.
- [46] F.C. Stedile, I.J.R. Baumvol, I.F. Oppenheim, I. Trimaille, J.-J. Ganem, S. Rigo, *Nucl. Inst. Meth. B118* (1996) 493.
- [47] R.J. Culbertson, Y. Kuk, L.C. Feldman, *Surf. Sci.* 167 (1986) 127.
- [48] K.T. Queeney, N. Herbots, et al., unpublished results.
- [49] R. Buczko, S.J. Pennycook, S.T. Pantelides, *Phys. Rev. Lett.* 84 (5) (2000) 943.
- [50] T. Schroeder, M. Adelt, B. Richter, M. Naschitzki, M. Baumer, H.-J. Freund, *Microelectr. Reliability* 40 (2000) 841.
- [51] T. Schroeder, M. Adelt, B. Richter, M. Naschitzki, M. Baumer, H.-J. Freund, *Surf. Rev. Lett.* 7 (1–2) (2000) 7.
- [52] T. Schroeder, A. Hammoudeh, M. Pykavy, N. Magg, M. Adelt, M. Baumer, H.-J. Freund, *Solid State Electr.*, in press.
- [53] S. Hahn, F.A. Ponce, W.A. Tiller, V. Stojanoff, D.A.P. Bulla, W.E. Castro Jr., *J. Appl. Phys.* 64 (9) (1988) 4454.